

Direct detection of polar structure formation in helium nanodroplets by beam deflection measurements

John W. Niman,^[a] Benjamin S. Kameron,^[a] Lorenz Kranabetter,^[b] Daniel J. Merthe,^{[a],†}
 Jiří Suchan,^[c] Petr Slaviček,^{*,[c,d]} Vitaly V. Kresin^{*,[a]}

^[a] *Department of Physics and Astronomy, University of Southern California,
Los Angeles, CA 90089-0484, USA*

^[b] *Institut für Ionenphysik und Angewandte Physik, Universität Innsbruck,
Technikerstr. 25, A-6020 Innsbruck, Austria*

^[c] *Department of Physical Chemistry, University of Chemistry and Technology,
Technická 5, Prague 6, Czech Republic*

^[d] *J. Heyrovský Institute of Physical Chemistry v.v.i., The Czech Academy of Sciences,
Dolejškova 3, 18223 Prague, Czech Republic*

Abstract

Long-range intermolecular forces are able to steer polar molecules submerged in superfluid helium nanodroplets into highly polar metastable configurations. We demonstrate that the presence of such special structures can be identified, in a direct and determinative way, by electrostatic deflection of the doped nanodroplet beam. The measurement also establishes the structures' electric dipole moments. In consequence, the introduced approach is complementary to spectroscopic studies of low-temperature molecular assembly reactions. It is enabled by the fact that within the cold superfluid matrix the molecular dipoles become nearly completely oriented by the applied electric field. As a result, the massive (tens of thousands of helium atoms) nanodroplets undergo significant deflections. The method is illustrated here by an application to dimers and trimers of dimethyl sulfoxide (DMSO) molecules. We interpret the experimental results with *ab initio* theory, mapping the potential energy surface of DMSO complexes and simulating their low temperature aggregation dynamics.

Introduction

Long-range intermolecular forces play an essential role in reactions at sub-Kelvin temperatures (see, e.g., the reviews in refs [1-4]). For example, long-range interactions between polar molecules embedded in helium nanodroplets often dominate the outcome of their assembly reactions. This is facilitated by the low internal temperature (370 mK) of the nanodroplet medium as well as by its superfluidity.^[5] As a result, molecular reorientation and intermolecular reactions within nanodroplets are not perturbed by inhomogeneities present in other low-temperature surface and matrix isolation environments, making these “nano-cryo-traps” excellent hosts for exploring the physics and chemistry of cold molecular systems.^[6]

A landmark demonstration of the action of long-range forces was furnished by experiments on HCN molecules sequentially picked up by a He nanodroplet beam.^[7] These linear molecules were guided by dipole-dipole forces to self-assemble into long chains aligned head-to-tail inside the nanodroplet. HCCCN was found to behave similarly.^[8] These chains rank among the most polar molecular systems ever observed in a molecular beam. In an “ordinary” environment thermal motion would drive them out of this type of metastable configuration, but within a very cold and inert liquid helium droplet they become long-lived. Data on formic acid,^[9] imidazole,^[10] and acetic acid^[11,12] dimers suggested an analogous alignment mechanism.

However, such an outcome is not universal in nanodroplet embedding. For example, two HCl molecules arrange themselves nearly at a right angle to each other^[13,14] while water clusters form cyclic structures.^[15] The “decision” by polar molecules how to orient themselves upon approach depends on the strength of their dipoles, on their responsiveness to the mutually reorienting torques (i.e., their rotational constants and their accessible rotational quantum states), and on the directionality and flexibility of their bond formation. That is to say, the outcome depends on the shape of the intermolecular potential energy surface and on the barrier

heights encountered on the path to the final configuration.

It is therefore interesting and informative to establish whether a molecular formation within a nanodroplet can reach its global energy minimum or finds itself trapped in a polar metastable state. However, often this is not a straightforward determination. The studies cited above based their conclusions on the interpretation of dopant infrared spectra or on inference from electron attachment mass spectrometry. Such assignments grow more difficult and less definitive with increasing size and/or complexity of the embedded molecules and their assemblies.

In this work we describe a measurement which *directly* establishes the polarity of a molecular assembly, as well as determines its dipole moment. It makes use of electrostatic deflection of the doped nanodroplet beam.^[16,17]

The technique is based on the fact that polar structures embedded within the superfluid matrix can be made nearly fully oriented by an external static electric field^[18] and consequently experience an extremely large deflecting force from the field's gradient. Such a high degree of orientation is unattainable for bare polyatomic complexes in a molecular beam. Whereas some relatively small and light molecules reach rotational temperatures T_{rot} below 1 K with the use of seeded supersonic expansions and exhibit large deflections (see, e.g., refs [19,20]), this becomes impractical for heavier systems.

For the purpose of an estimate, consider the classical Langevin function for the orientation of a molecular rotor in an external field $E\hat{z}$: $\bar{p}_z/p_0 = [\coth x - 1/x]$. This is a good approximation^[21,22] for $k_B T_{rot} \gg B$. Here p_0 is the molecule's dipole moment, \bar{p}_z is the average projection of this dipole on the field axis, $x \equiv p_0 E / k_B T_{rot}$, and B is the rotational constant. For T_{rot} above a few K and practical electric field strengths, the ratio x remains small even for dipole moments of several Debye (D), and in this limit $\bar{p}_z/p_0 \approx x/3 \ll 1$. Therefore it is only when

the rotational temperature becomes very low, as enabled in the present case by helium nanodroplet isolation, that the orientation can approach saturation ($\bar{p}_z \rightarrow p_0$). This effect has been taken advantage of in landmark experiments using pendular-state spectroscopy.^[18]

If the external electric field which orients the nanodroplet-submerged dipoles is designed also to have a strong gradient in the same direction, then these dipoles will experience such a strong sideways force $F_z = p_z (\partial E / \partial z)$ that the massive doped droplets, comprised of tens of thousands of helium atoms, will be significantly deflected in their entirety. Thus, our procedure involves comparing the deflection profile of a singly-doped nanodroplet beam with that of a beam composed of multiply-doped nanodroplets. If, for example, the droplets containing two (or three, etc.) molecules show negligible deflection, we can immediately conclude that the dimer (trimer, etc.) has settled into a nonpolar configuration. A strongly deflected profile, on the other hand, immediately attests to the formation of a polar structure, and the magnitude of the deflection translates into the magnitude of this formation's total dipole moment.

This is a conveniently unambiguous measurement applicable to a wide range of molecules, from diatomic to polyatomic (including biological). Practically any molecular species that can be brought into the vapor phase with a pressure of only 10^{-6} - 10^{-4} mbar can be picked up by the nanodroplet beam and thermalized within the inert viscosity-free medium. The thermalization proceeds by evaporative cooling: the molecules' translational and internal energies are transferred to the superfluid matrix which has a very high thermal conductivity, and released via evaporation of surface helium atoms, promptly bringing the nanodroplet back to the original temperature.^[5]

Here we apply the deflection method to monomers, dimers and trimers of the dimethyl sulfoxide molecule ("DMSO," $(\text{CH}_3)_2\text{SO}$, molecular mass 78 Da). The molecule is nearly an oblate symmetric top, with rotational constants of^[23,24] 0.235 cm^{-1} , 0.231 cm^{-1} , and 0.141 cm^{-1}

and its total dipole moment is^[25] $p=4.0$ D. The measurement clearly reveals the presence of highly polar dimers and trimers, i.e., the formation of metastable polar configurations abetted by the cryogenic nanodroplet environment. To our knowledge, this is the first direct non-spectroscopic identification of such a cold polar molecular assembly.

Results and Discussion

Deflection profiles. The experimental setup has been described in detail elsewhere.^[16,17,26] A nanodroplet beam is formed by cold nozzle expansion of pure helium gas. It passes first through a pick-up cell filled with DMSO vapor, and then between two high-voltage electrodes which create an electric field and a collinear field gradient directed perpendicular to the beam axis. Downstream, the beam enters through a slit into an electron-impact ionizer, and the intensities of the resulting molecular ions are recorded by a quadrupole mass spectrometer in synchronization with a beam chopper. The deflection induced by the electric field is determined by comparing the beam's "field-on" and "field-off" spatial profiles which are mapped out by translating the detector chamber, with its entrance slit, on a precision linear stage.

Molecules are picked up by helium nanodroplets via successive collisions in a Poisson process.^[5] Therefore it is important to correlate measured beam deflections with the specific number of molecules embedded in the droplet. In other words, when mapping out the deflection profile of a dopant ion peak in the mass spectrum, we need to ensure that it is not a fragment of a larger agglomerate. This is done by gradually increasing the vapor pressure in the pick-up cell and monitoring the mass spectrum for the appearance of molecular ions characteristic of progressively larger entities. For example, monomer ionization produces a strong $(\text{DMSO})^+$ signal^[27] at $m=78$ Da, hence if we measure beam profiles with the mass spectrometer set to this mass peak but with the vapor pressure low enough to suppress the corresponding characteristic

(DMSO)₂⁺ peak at $m=156$ Da, then we can be confident that the deflection principally corresponds to droplets carrying the monomer. Similarly, profiles measured at $m=156$ Da but before the appearance of the trimer's signal must derive from the dimer, etc. Representative mass spectra are shown in the Supporting Information (SI).

Fig. 1 shows the deflection profiles of helium nanodroplets containing one, two, and three DMSO molecules. The deflections are substantial despite the fact that the droplets are truly massive ($\sim 1 \times 10^4$ – 3×10^4 He atoms, as described in the caption). Therefore we are immediately and directly informed by Fig. 1(b) that (DMSO)₂ settles into a strongly polar configuration and not into its global minimum structure, because the latter would be symmetric with a zero dipole moment.^[28]

In order to assign an absolute value of the dipole moment to the dopant, we must keep in mind that the host nanodroplets are not all of the same size. The size distribution produced by the nozzle expansion is log-normal, and this translates into a convolution of pick-up cross sections, deflection angles, and ionization efficiencies. Our procedure^[16,17] is to start with the profile corresponding to a single DMSO dopant molecule whose dipole moment is known. A fit to the deflected profile (by a Monte Carlo simulation of the pick-up, evaporation, deflection, and detection steps) is used to calibrate the droplet size distribution. Then by repeating the deflection measurement and its simulation with doubly- and triply-doped nanodroplets produced and detected under the same conditions, we can deduce the electric dipole moments corresponding to the dimer and the trimer.

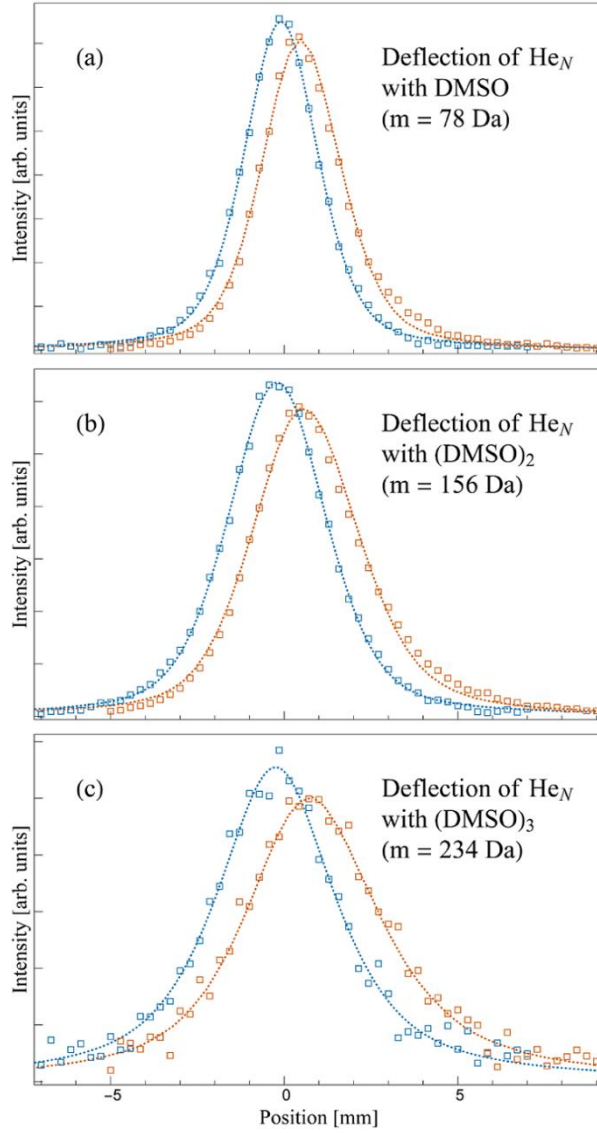


Figure 1. Profiles of $(\text{DMSO})_n$ -doped helium nanodroplet beams. Blue: zero-field profiles, orange: deflection by a field of 82 kV/cm strength and 338 kV/cm^2 gradient. Symbols: experimental data, lines: fits of the deflection process, as described in the text. The monomer profile mapped for a particular temperature T and stagnation pressure P of the He_N beam source is used to determine the average \bar{N} and width ΔN of the nanodroplet size distribution, and then fits to the dimer and trimer profiles for the same source conditions yield these dopants' dipole moments. In (b) $P=80 \text{ bar}$, $T=15.5 \text{ K}$, $\bar{N} \approx 2.3 \times 10^4$, in (c) $P=80 \text{ bar}$, $T=16.4 \text{ K}$, $\bar{N} \approx 1.4 \times 10^4$.

These dipole moments enter the fitting procedure at the step where the deflecting electrostatic force is calculated. As described in the Introduction, this requires knowing \bar{p}_z , i.e., the degree of orientation induced by the applied field. For the DMSO monomer this is carried out by diagonalizing the rotational Stark effect matrix (cf. ref [29]) using the components of the molecule's dipole moment.^[24] For the heavier dimer and trimer the classical Langevin-Debye formula is sufficiently accurate.^[30] In calculating the monomer's Stark spectra one should keep in mind that rotational coupling to the superfluid^[31] enhances the moments of inertia of the heavier molecular rotors by an average factor of $\sim 2.5-3$ compared with their gas phase value.^{5,18} Since DMSO's specific renormalization factor is not known, it was set to 2.6 in our data fitting procedure. We found that the inclusion of this factor had practically no effect on the deduced dipole of the dimer but shifted that of the trimer upward by $\approx 10\%-15\%$. For the final fitted dipole values listed below, the $(\text{DMSO})_n$ orientations within an applied 82 kV/cm field were found to be 86%, 97%, and 98% for $n=1-3$, respectively.

Dipole moments. From analysis of the measurements, we assign effective electric dipole moments of 7.2 D to $(\text{DMSO})_2$ and 8.6 D to $(\text{DMSO})_3$, with an estimated accuracy of ± 0.2 D and ± 0.6 D, respectively. These values, which can be compared with the ground state moments of 0 D for the aforementioned symmetric dimer and 4.2 D for the trimer^[28] (essentially a nonpolar dimer plus an unpaired monomer), establish the presence of highly polar metastable structures. In the cold superfluid environment these structures are steered into formation by the long-range intermolecular forces and are then unable to overcome the potential barrier leading to the global minimum configuration.

Modeling of molecular complex formation. To facilitate the interpretation of the above results, we supplemented the experiments with *ab initio* modeling of DMSO condensation. We optimized the geometry of DMSO dimers and trimers with the B3LYP functional with the aug-

cc-pVDZ basis set. The DMSO complexes are dominantly bound by electrostatic forces but the dispersion interactions still play a non-negligible role. We have therefore used the D2 correction of Grimme.^[32] The approach was tested against the CCSD(T)/aug-cc-pVTZ method for the DMSO dimer, yielding similar energetics (see the SI). All calculations were performed in the gas phase: by considering complexes with helium atoms or within a dielectric continuum we found that the helium environment had a negligible effect on the structure and energetics. The potential energy surfaces (PES) were pre-screened with molecular mechanics (MM)-based metadynamics simulations^[33] and the structures were then recalculated at the DFT level (see the SI for further information).

The process of DMSO dimer formation was modeled with molecular dynamics (MD) simulations within the canonical ensemble. We used the Nosé-Hoover thermostat with a rather small value of $\tau = 0.01$ ps. This corresponds to fast draining of extra energy from the system, so that at each time it essentially remains in equilibrium. A temperature of 5 K was chosen in order to accelerate the simulations. It is higher than in the experiment but the difference is small compared with the PES accuracy.

We started with two DMSO molecules positioned at a distance of 20 Å between the two sulphur atoms with a random orientation. We then performed molecular mechanics simulations with the MM force field.^[34] The molecules gradually approached each other while aligning their dipole moment. Since the MM force field does not reproduce the energetics of the minima sufficiently well, at the intermolecular distance of 10 Å we reset the simulations, switching from the force field to the more accurate semiempirical density functional tight binding (DFTB) method^[35] with D3 dispersion correction.^[36,37] The system then continued to evolve in time for another 500 ps with a time step of 1 fs, using the velocity Verlet integrator. Dipoles along the path were recalculated at the B3LYP/aug-cc-pVDZ level.

The DFT and CCSD(T) calculations were performed in Gaussian09.^[38] Molecular dynamics simulations were performed in GROMACS 2018.4^[39] and the DFTB simulations in the DFTB+ 18.2 code.^[35] We also utilized our in-house MD code ABIN.^[40]

Results of modeling. Fig. 2 shows several low-lying minima of the DMSO dimer obtained from extensive mapping of its potential energy surface. The structures are divided into two classes of minima: non-polar and polar. The global minimum (complex D1) of (DMSO)₂ has a symmetrical configuration with a zero dipole moment, consistent with the aforementioned work.^[28] Structures D2 and D3 also belong to the low dipole manifold. Complexes D4 and D5 represent polar type structures. The experimental data suggest that the highly polar structure D5, with an almost orthogonal arrangement of dipoles, predominantly forms within nanodroplets. It is separated from the global minimum by a barrier of 0.08 eV (see the SI), which is more than sufficient to prevent a D5 → D1 transition.

Structure formation under cryogenic conditions is therefore likely to proceed as follows. At large separation the dominant force is the dipole-dipole interaction which aligns the two DMSO molecules. As described in the SI, there is a barrierless pathway between this structure and the D5 minimum. Therefore the molecules approach each other gradually within the helium environment to which all excess energy is almost immediately drained. The (DMSO)₂ ends up trapped within the basin of complex D5.

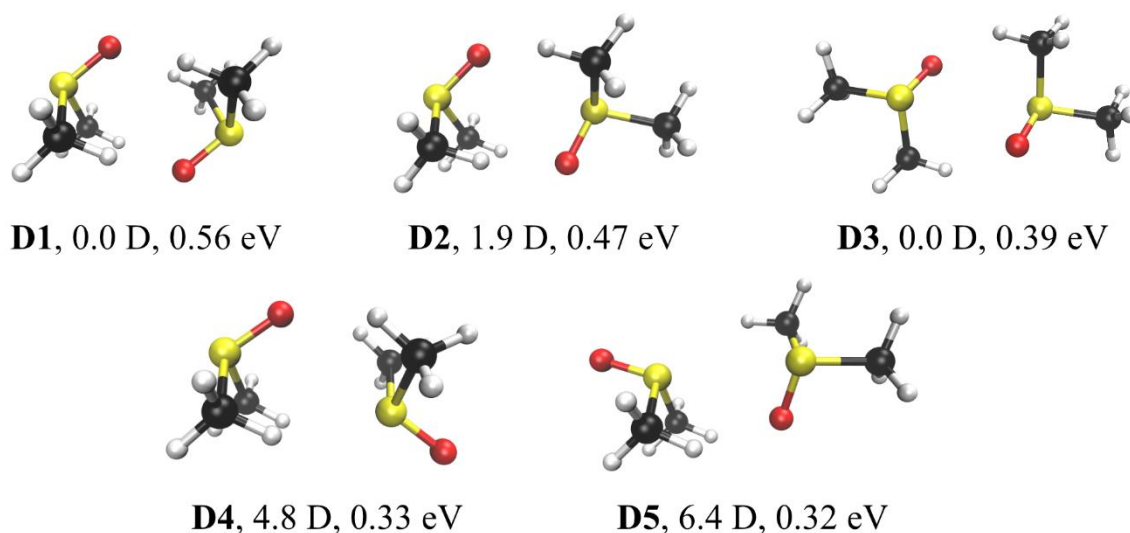


Figure 2. Energy minima of the DMSO dimer, with their corresponding binding energies and dipole moments.

We support this scenario by molecular dynamics (MD) simulations of the binary encounter under conditions of very efficient energy transfer. At the start the two dipoles are assigned a random relative orientation, but the trajectory shown in Fig. 3 demonstrates that it becomes correlated already at large distances. At closer approach the total dipole moment transiently increases. The molecular dipoles at that point are still parallel, hence the bump in the dipole moment is caused by mutual induction. Finally, the dimer quenches into one of the potential minima. In accord with the experiment, no formation of a zero dipole structure is found. The majority of the trajectories end up in the D5 minimum with a dipole of 6.4 D, some of them end up in the D4 minimum with a somewhat lower dipole moment than detected in the experiment.

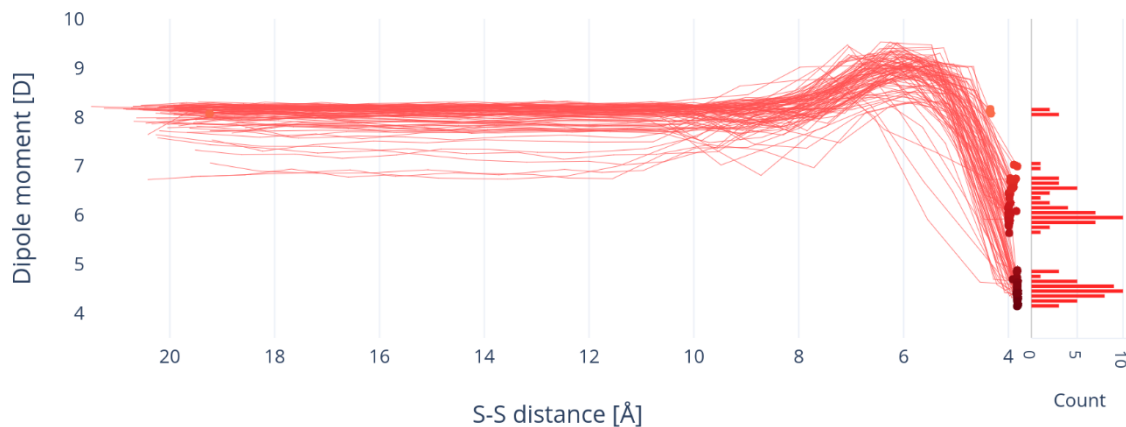


Figure 3. Dipole moment of DMSO dimer complex along the intermolecular approach coordinate, as illustrated by a molecular dynamics simulation.

The structures are more diverse for the trimer (Fig. 4). The lowest energy structure is cyclic with a dipole moment of 4.25 D (complex T1). Its formation is kinetically hindered. Indeed, as mentioned above, it represents the global dimer minimum to which the third molecule is added; since in the nanodroplets the former structure is not formed, neither will the cyclic trimer. We have located linear structures (T6, T7) with a much higher dipole close to 10 D. There are multiple other minima with intermediate dipoles. It follows from our simulations that a rather complex mixture of these metastable structures may be formed under the experimental conditions, and its precise assignment is beyond the reach of theory. The effective dipole moment of ≈ 8.6 D deduced from the deflection experiment represents the population average of the kinetically accessible structures.

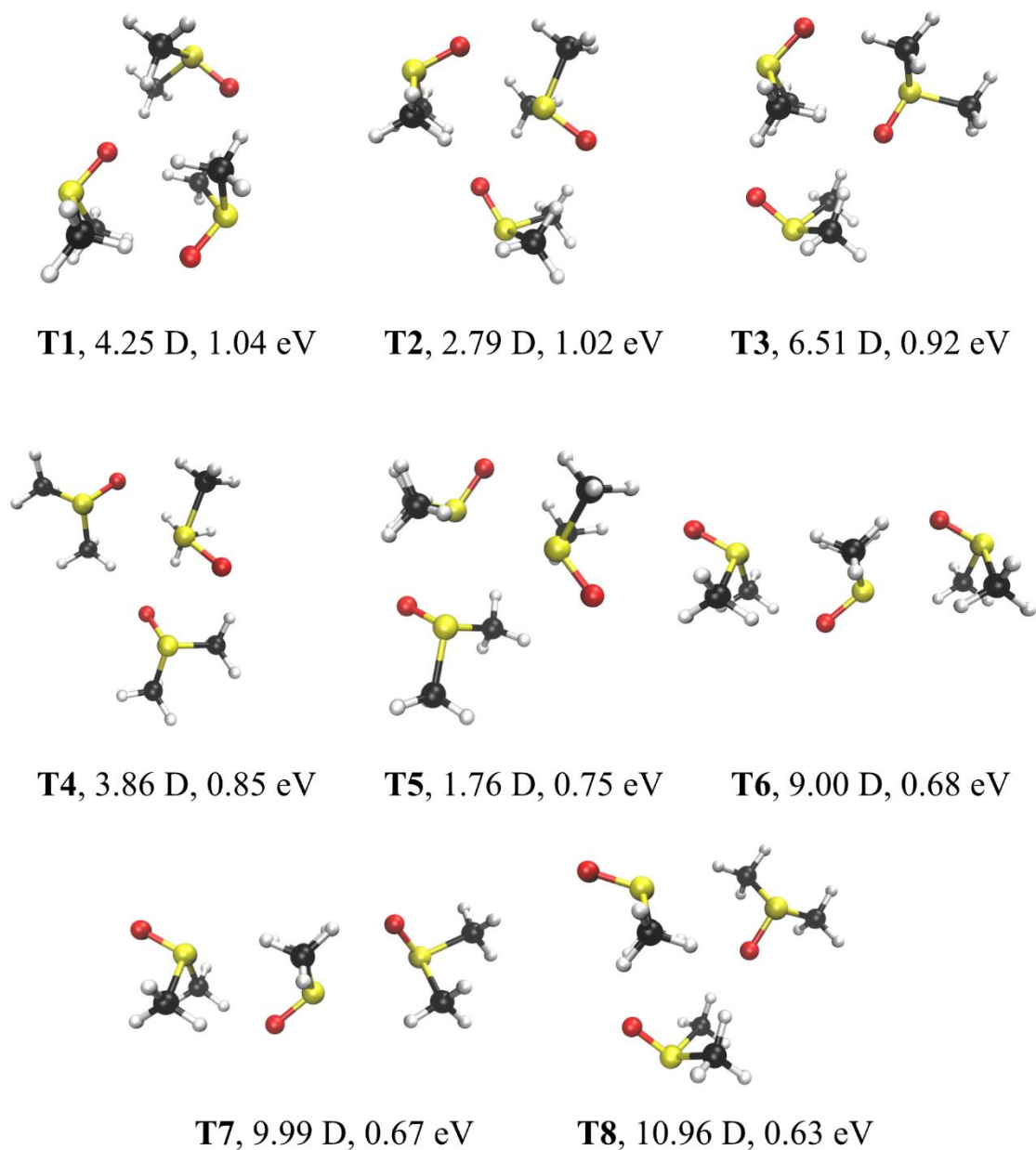


Figure 4. Energy minima of DMSO trimers, with their corresponding binding energies and dipole moments.

Conclusion

In summary, we have demonstrated that the presence of peculiar polar structures, formed by sequential embedding of polar molecules into superfluid helium nanodroplets, can be clearly and directly detected by electrostatic deflection of the doped nanodroplet beam. In an

application of this method to DMSO molecules we found that they form dipole-aligned dimer and trimer structures, steered by long-range electrostatic interactions. The formation mechanism and the magnitudes of the dipole moments are in good agreement with calculations describing molecular interactions and structure formation in the viscosity-free cryogenic environment.

In future applications it will be interesting to extend this approach, for example, to a study of interactions between polar amino acids or between prototype solute and solvent molecules, as well as between molecules in photoinduced polar conformations. It is also interesting to inquire whether transfer of angular momentum between the impurities and the quantum-fluid bath, a phenomenon predicted to have the potential to screen the impurity – electric field interaction,^[41] may be able to measurably affect the dynamics of molecular assembly within nanodroplets.

Acknowledgments

This work was supported by the U. S. National Science Foundation under Grant No. CHE-1664601. L.K. acknowledges a scholarship from the Austrian Marshall Plan Foundation and support from the Austrian Science Fund under project FWF W1259. J.S. and P.S. thank the Czech Science Foundation for support under Project number 18-16577S. J.S. is an International Max Planck Research School for Many Particle Systems in Structured Environments student. We would like to thank Jiahao Liang and Atef Sheekhoon for assistance.

References

- [1] M. T. Bell, T. P. Softley, *Mol. Phys.* **2009**, *107*, 99-132.
- [2] M. Schnell, G. Meijer, *Angew. Chem. Int. Ed.* **2009**, *48*, 6010-6031.
- [3] G. Quéméner, P. S. Julienne, *Chem. Rev.* **2012**, *112*, 4949-5011.
- [4] N. Balakrishnan, *J. Chem. Phys.* **2016**, *145*, 150901.
- [5] J. P. Toennies, A. F. Vilesov, *Angew. Chem. Int. Ed.* **2004**, *43*, 2622-2648.
- [6] K. K. Lehmann, G. Scoles, *Science* **1998**, *279*, 2065-2066.
- [7] K. Nauta, R. E. Miller, *Science*. **1999**, *283*, 1895-1897.
- [8] K. Nauta, D. T. Moore, R. E. Miller, *Faraday Discuss.* **1999**, *113*, 261-278.
- [9] F. Madeja, M. Havenith, K. Nauta, R. E. Miller, J. Chocholoušová, P. J. Hobza, *Chem. Phys.* **2004**, *120*, 10554-10560.
- [10] M. Y. Choi, R. E. Miller, *J. Phys. Chem. A.* **2006**, *110*, 9344-9351.
- [11] F. Ferreira da Silva, S. Jaksch, G. Martins, H. M. Dang, M. Dampc, S. Denifl, T. D. Märk, P. Limão-Vieira, J. Liu, S. Yang, A. M. Ellis, P. Scheier, *Phys. Chem. Chem. Phys.* **2009**, *11*, 11631-11637.
- [12] J. A. Davies, M. W. D. Hanson-Heine, N. A. Besley, A. Shirley, J. Trowers, S. Yang, A. M. Ellis, *Phys. Chem. Chem. Phys.* **2019**, *21*, 13950-13958.
- [13] M. Ortlieb, Ö. Birer, M. Letzner, G. W. Schwaab, M. Havenith, *J. Phys. Chem. A.* **2007**, *111*, 12192-12199.
- [14] D. Skvortsov, R. Sliter, M. Y. Choi, A. F. Vilesov, *J. Chem. Phys.* **2007**, *128*, 094308.
- [15] K. Nauta, R. E. Miller, *Science*. **2000**, *287*, 293-295.

- [16] D. J. Merthe, V. V. Kresin, *J. Phys. Chem. Lett.* **2016**, *7*, 4879-4883.
- [17] J. W. Niman, B. S. Kamerin, D. J. Merthe, L. Kranabetter, V. V. Kresin, *Phys. Rev. Lett.*, in press (July 2019).
- [18] M. Y. Choi, G. E. Douberly, T. M. Falconer, Lewis, W. K. Lewis, C. M. Lindsay, J. M. Merritt, P. L. Stiles, R. E. Miller, *Int. Rev. Phys. Chem.* **2006**, *25*, 15-75.
- [19] Y.-P. Chang, D. Horke, S. Trippel, J. Küpper, *Int. Rev. Phys. Chem.* **2015**, *34*, 557-590.
- [20] M. Johny, J. Onvlee, T. Kierspel, H. Bieker, S. Trippel, J. Küpper, *Chem. Phys. Lett.* **2019**, *721*, 149-152.
- [21] B. Friedrich, D. Herschbach, *Int. Rev. Phys. Chem.* **1996**, *15*, 325-344.
- [22] J. Bulthuis, J. A. Becker, R. Moro, V. V. Kresin, *J. Chem. Phys.* **2008**, *129*, 024101.
- [23] W. Feder, H. Dreizler, H. D. Rudolph, V. Typke, *Z. Naturforsch.* **1969**, *24a*, 266-278.
- [24] M. L. Senent, S. Dalbouha, A. Cuisset, D. Sadovskii, *J. Phys. Chem. A.* **2015**, *119*, 9644-9652.
- [25] *CRC Handbook of Chemistry and Physics*, 99th ed. (Ed.: J. R. Rumble), CRC Press, Boca Raton, **2018**.
- [26] D. J. Merthe, PhD dissertation, University of Southern California (Los Angeles), **2017**.
- [27] *NIST Chemistry WebBook, NIST Standard Reference Database Number 69* (Eds.: P. J. Linstrom, W. G. Mallard), National Institute of Standards and Technology, Gaithersburg, **2018**. <http://webbook.nist.gov>.
- [28] N. S. Venkataramanan, A. Suvitha, Y. Kawazoe, *J. Mol. Liq.* **2018**, *249*, 454-462.
- [29] Y.-P. Chang, F. Filsinger, B. G. Sartakov, J. Küpper, *Comput. Phys. Commun.* **2014**, *185*, 339-349.

- [30] L. Pei, J. Zhang, W. Kong, *J. Chem. Phys.* **2007**, *127*, 174308.
- [31] M. Lemeshko, *Phys. Rev. Lett.* **2017**, *118*, 095301.
- [32] S. Grimme, *J. Comput. Chem.* **2006**, *27*, 1787-1799.
- [33] A. Barducci, M. Bonomi, M. Parrinello, *WIREs Comput. Mol. Sci.* **2011**, *1*, 826-843.
- [34] M. L. Strader, S. E. Feller, *J. Phys. Chem. A.* **2002**, *106*, 1074-1080.
- [35] B. Aradi, B. Hourahine, Th. Frauenheim, *J. Phys. Chem. A.* **2007**, *111*, 5678-5684.
- [36] S. Grimme, J. Antony, S. Ehrlich, H. Krieg, *J. Chem. Phys.* **2010**, *132*, 154104.
- [37] S. Grimme, S. Ehrlich, L. Goerigk, *J. Comput. Chem.* **2011**, *32*, 1456-1465.
- [38] M. J. Frisch *et al.* *Gaussian 09, rev D.01*, Gaussian, Inc., Wallingford (CT), **2009**.
- [39] M. J. Abraham, T. Murtola, R. Schulz, S. Páll, J. C. Smith, B. Hess, E. Lindahl, *SoftwareX.* **2015**, *1-2*, 19-25.
- [40] *ABIN, Molecular Dynamics program*. Source code available at <https://github.com/photox/abin>. doi:10.5281/zenodo.1228462.
- [41] E. Yakaboylu, M. Lemeshko, *Phys. Rev. Lett.* **2017**, *118*, 085302.

**Direct detection of polar structure formation in helium nanodroplets
by beam deflection measurements**

John W. Niman,^[a] Benjamin S. Kamerin,^[a] Lorenz Kranabetter,^[b] Daniel J. Merthe,^[a]
Jiří Suchan,^[c] Petr Slavíček,^[c,d] Vitaly V. Kresin^[a]

^[a] *Department of Physics and Astronomy, University of Southern California,
Los Angeles, CA 90089-0484, USA*

^[b] *Institut für Ionenphysik und Angewandte Physik, Universität Innsbruck,
Technikerstr. 25, A-6020 Innsbruck, Austria*

^[c] *Department of Physical Chemistry, University of Chemistry and Technology,
Technická 5, Prague 6, Czech Republic*

^[d] *J. Heyrovský Institute of Physical Chemistry v.v.i., The Czech Academy of Sciences,
Dolejškova 3, 18223 Prague, Czech Republic*

Contents

- I. (DMSO)_n ion mass spectra
 - II. Ab initio calculations: Benchmarking
 - III. Mapping of the (DMSO)₂ and (DMSO)₃ potential energy surfaces
 - IV. Transition between two dimers at a distance and D5
 - V. Transition between the D5 and D1 minima
 - VI. Two dimensional free energy surface
 - VII. Force field parameters
 - VIII. Cartesian coordinates of all structures
- References

I. (DMSO)_n ion mass spectra

As described in the main text, deflection profiles of droplets doped with DMSO monomers, dimers, or trimers were acquired by setting the mass spectrometer to the masses of (DMSO)⁺, (DMSO)₂⁺ and (DMSO)₃⁺ ions, respectively, and maintaining the pickup vapor pressure at a level such that the mass peak of interest would be dominant over the next higher one. This is illustrated in Fig. S1. The mass spectrometer is a Balzers QMG-511 crossed-beam quadrupole analyzer with its electron impact ionization source set to 90 eV impact energy.

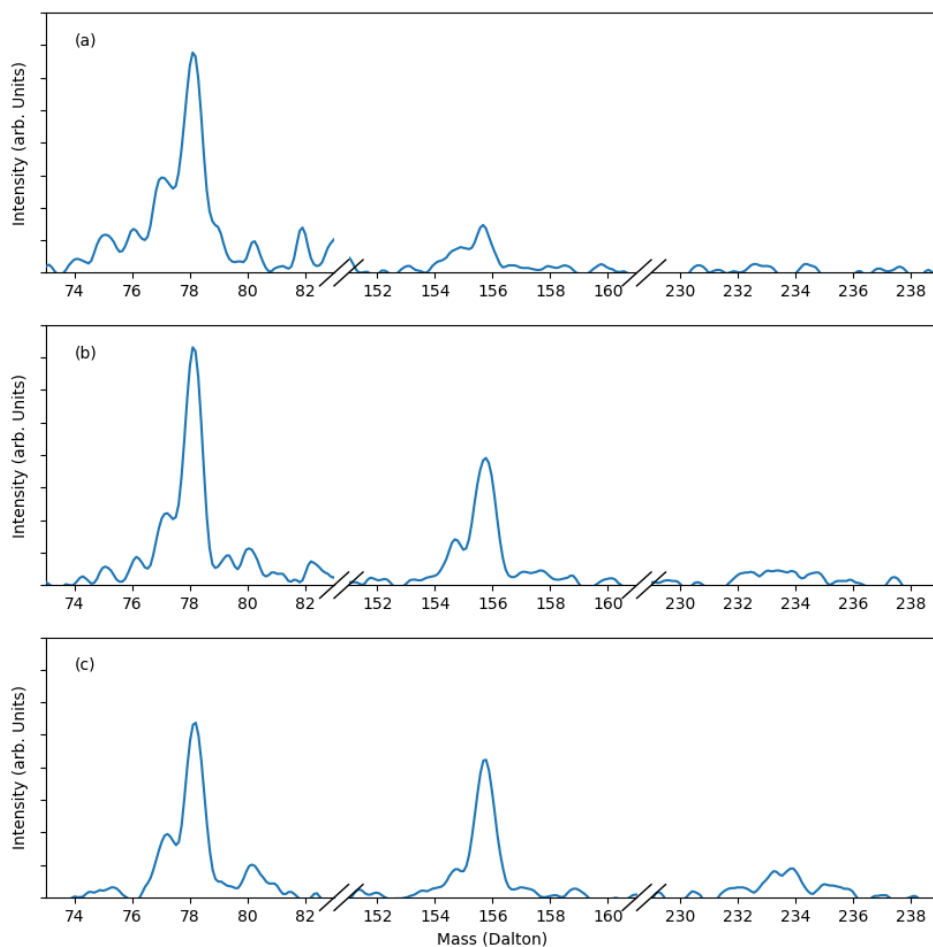


Figure S1. Representative mass spectra corresponding to deflection measurements on (DMSO)_n-doped nanodroplets. The mass spectrometer was set to the masses of intact ions: (a) 78 Da for the monomer, (b) 156 Da for the dimer, (c) 234 Da for the trimer.

II. Ab initio calculations: Benchmarking

The potential energy surface was explored with the B3LYP(D2)/aug-cc-pVDZ method. The dipole moment of the isolated DMSO molecule in its equilibrium geometry calculated with this approach was 4.3 D, which is consistent with the tabulated value^[S1] of 4.0 D within the expected accuracy of DFT.^[S2] We validated this approach against the high-level CCSD(T)/aug-cc-pVTZ method. Basis set superposition error (BSSE) correction was used for all structures. The agreement is very good for all cluster structures, see Table S1. We also show the energetics of the respective minima at the DFTB/D3 level used for exploratory simulations. The DFT and CCSD(T) calculations were performed in the Gaussian 09, rev. D01 package,^[S3] the DFTB results were calculated in the DFTB+ 18.2 program.^[S4]

Table S1. Comparison of DMSO dimer binding energies at the CCSD(T), B3LYP(D2) and DFTB(D3) levels. The BSSE correction was accounted for in the CCSD(T) and B3LYP(D2) calculations.

Dimer complex	Binding energy [eV]		
	CCSD(T)/aug-cc-pVTZ	B3LYP/aug-cc-pVDZ D2	DFTB
D1	0.53	0.56	0.46
D2	0.46	0.47	0.41
D3	0.40	0.39	0.36
D4	0.33	0.33	0.28
D5	0.32	0.32	0.26

III. Mapping of the (DMSO)₂ and (DMSO)₃ potential energy surfaces

The potential energy surfaces (PES) of DMSO complexes are rather rich and we mapped them in the following way. First, we performed accelerated molecular dynamics simulations with the molecular mechanics (MM) force field,^[S5] using the so-called metadynamics method.^[S6] Here, an additional potential is added along a preselected coordinate so that we can quickly overcome barriers along these coordinates. These simulations then also provide the free energy as a function of the selected coordinate [potential of mean force (PMF) or free energy surface (FES)]. We then selected different structures with distinct dipole moments from these metadynamical trajectories and performed further B3LYP optimization.

Metadynamics simulations were performed at 100 K to reveal the regions of interest in the dipole moment coordinate. This temperature is much higher than the experimental conditions, yet we opted for it to avoid ergodicity problems. Note that these simulations are only auxiliary, serving as a starting point for minimizations or MD simulations. The minimum on the PMF is found for a small yet non-zero dipole moment due to entropic reasons. The force field overestimates the dipole moment by 20% with respect to the *ab initio* value. The final PMFs for the dimer and trimer complexes are displayed in Fig. S2.

By clustering structures with similar dipoles together and performing 100 subsequent optimizations with Gaussian 09, for both the dimer and trimer structures, we were then able to map their PES landscapes.

The metadynamics parameters were as follows. The dimer simulation length was 100 ps, leap-frog stochastic integrator was utilized, the temperature was set to 100 K with a thermostat constant of $\tau = 1.0$ ps. For the trimer the simulation length was increased to 300 ps. The collective variable (CV) is the total dipole moment. An additional Gaussian potential was added every 100 steps. The Gaussian height was 0.015 kJ/mol and the CV gaussian width was 1.2 Debye.

MD simulations were performed with GROMACS 2018.4 code^[S7] coupled with PLUMED 2.5 code^[S8] for the FES simulations.

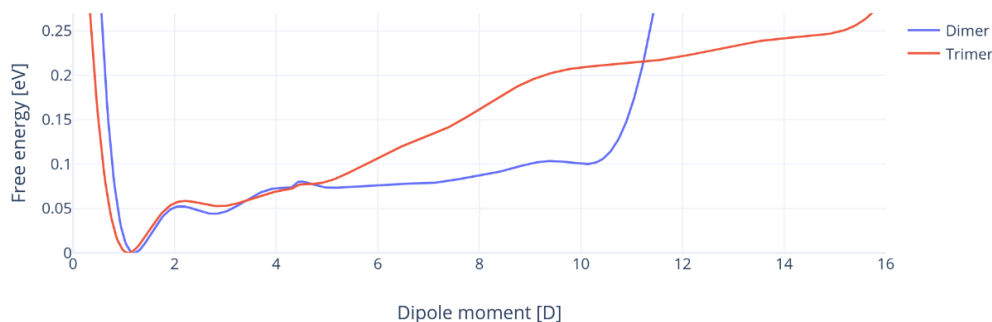


Figure S2. PMF for DMSO dimer and trimer complexes for the dipole moment coordinate at 100K.

IV. Transition between two dimers at a distance and D5

Nudged elastic band (NEB) optimization^[S9] was performed to find energy barriers between two DMSO molecules a distance apart (13.5 Å; in the minimal geometry at that separation the two DMSO molecules have aligned dipoles) and complex D5. Fig. S3 shows that the connection is barrierless.

The simulations were carried out in the TeraChem code^[S10,S11] using the B3LYP(D2)/aug-cc-pVDZ method with 14 molecular images between the two structures. The images were generated by constrained minimization.

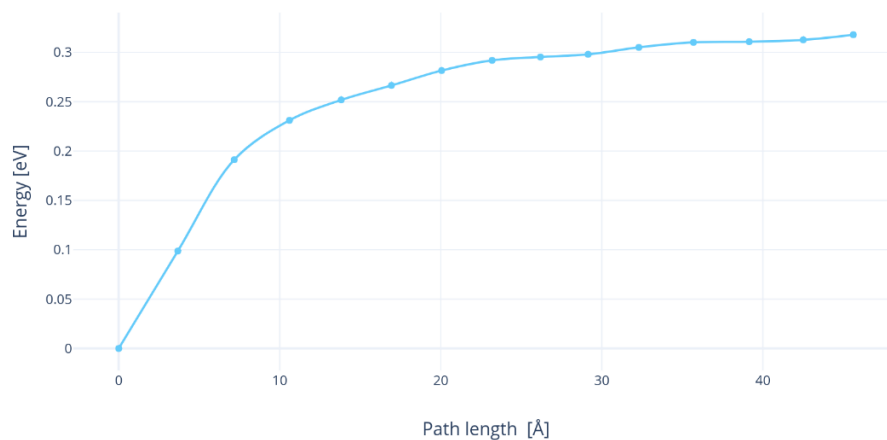


Figure S3. NEB calculations connecting the long-distance configuration to the D5 minimum.

V. Transition between the D5 and D1 minima

We also performed NEB calculation connecting the D5 minimum with the global D1 minimum. The final energy curve is shown in Fig. S4.

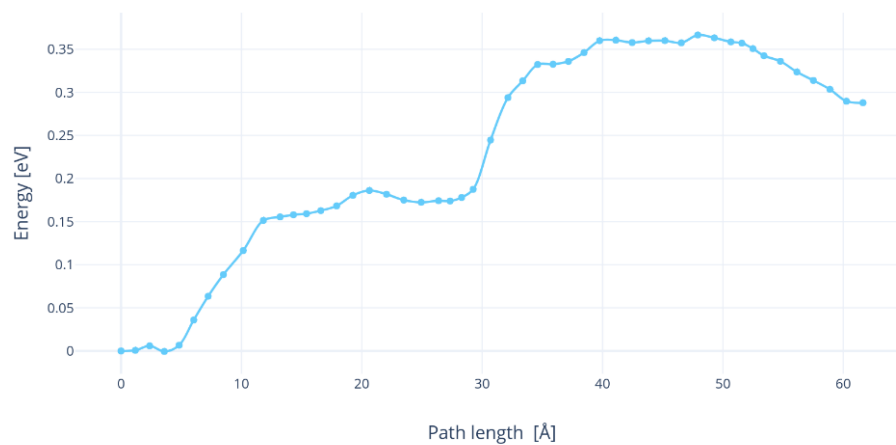


Figure S4. NEB calculations connecting the minima D1 and D5.

VI. Two dimensional free energy surface

Additional insight into the topology of the multidimensional PES of DMSO aggregates can be brought about via modeling of free energy surfaces (FES). We evaluated the FES (i.e., the two dimensional version of the PMF in Fig. S2) as a function of two coordinates: the aggregate dipole moment and the interatomic S-S distance, see Figs. S5-S8. The graphs were once again generated using the metadynamics method and the temperature of 100 K to avoid convergence issues. It is clear that at large intermolecular distance the system prefers the high-dipole configuration, as mentioned above. At close distances one observes a number of minima separated by barriers.

The 2D metadynamics parameters were as follows. As before, for the dimer the simulation length was 100 ps, leap-frog stochastic integrator was utilized, the temperature was set to 100 K with thermostat constant $\tau=1.0$ ps. The first collective variable, CV1, was defined as the S-S interatomic distance between the DMSO monomers. An additional Gaussian potential was added at every 1000 steps. The Gaussian height was 0.015 kJ/mol and the CV1 Gaussian width was 0.1 nm. The second collective variable was the dipole moment with the same deposition parameters as CV1 and Gaussian width of 1.2 D. Upper energetic walls for CV1 were applied at 2 nm in order to keep the molecule in the area of interest.

For the trimer the simulation length was increased tenfold to 1000 ps, with the other parameters fixed. CV1 was redefined as the sum of S-S interatomic distances due to the presence of the third DMSO molecule, the other variables remained the same. The upper energetic walls for CV1 were shifted to 6.0 nm.

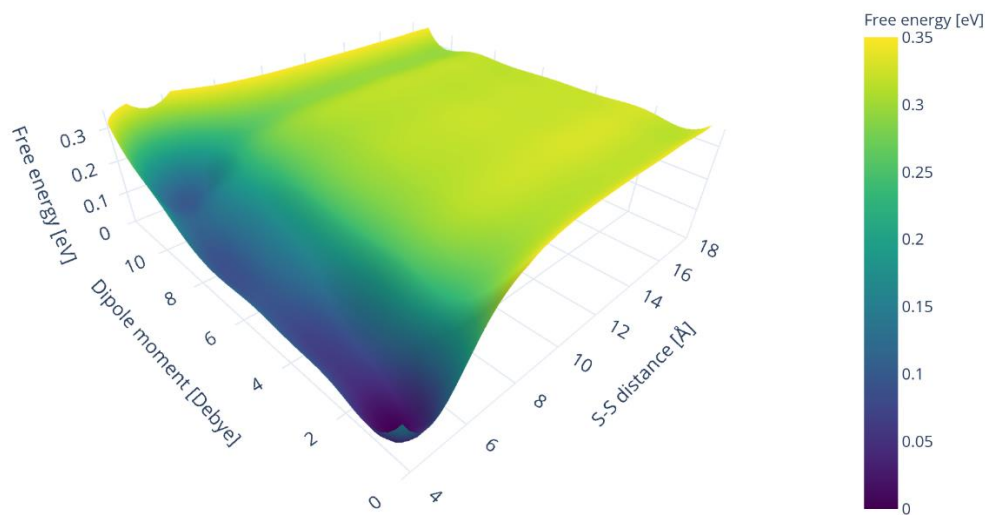


Figure S5. FES for the DMSO dimer at 100 K.

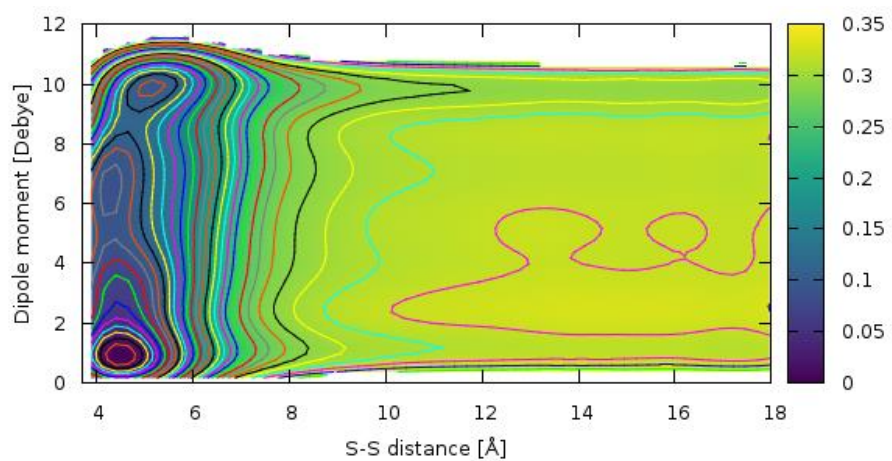


Figure S6. FES heatmap for the DMSO dimer at 100 K. Contour spacing 0.01 eV.

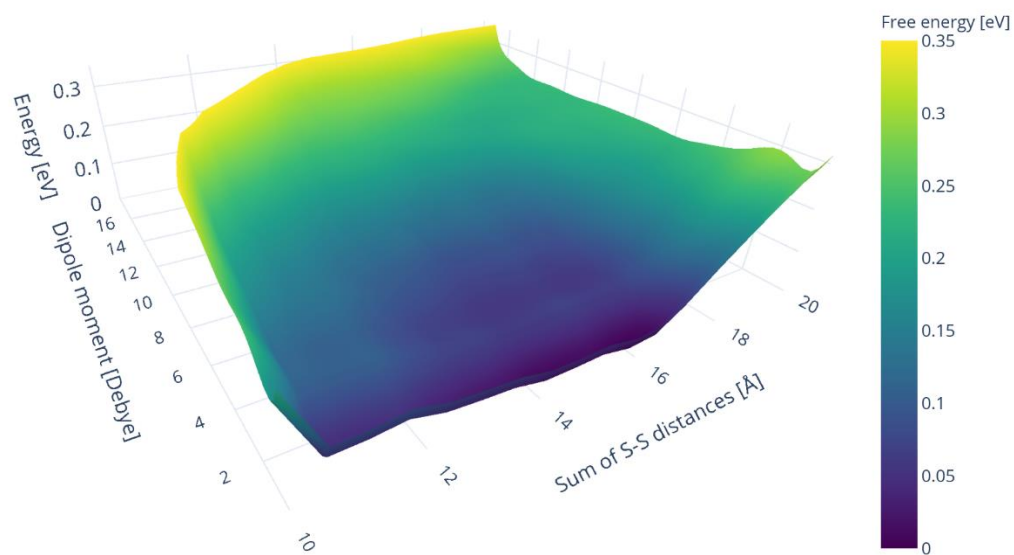


Figure S7. FES for the DMSO trimer at 100 K.

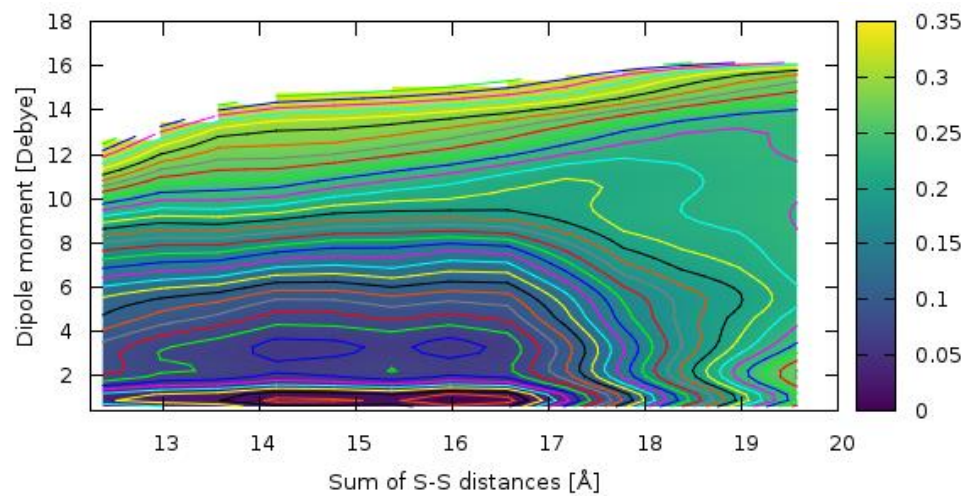


Figure S8. FES heatmap for the DMSO trimer at 100 K. Contour spacing 0.01 eV.

VII. Force field parameters

The MM simulations were performed with parameters taken from ref S5. The parameters are summarized in Tables S2 and S3.

Table S2. Atomic type parameters for DMSO.

Atom	Charge	ϵ (kJ/mol)	σ (nm)
O	-0.556	0.50242	0.30291
S	0.312	1.46537	0.35636
C	-0.148	0.32657	0.36348
H	0.090	0.10048	0.23876

Table S3. Intermolecular parameters for DMSO.

Bond	b_0 (nm)	f_c (kJ mol ⁻¹ nm ⁻²)
H-C	0.111	134724.8
C-S	0.180	100416.0
S-O	0.153	225936.0

Angles	θ_0 (nm)	f_c (kJ mol ⁻¹ rad ⁻²)
H-C-H	108.400	148.5320
H-C-S	111.300	192.8824
C-S-O	106.750	330.5360
C-S-C	95.000	142.2560

Dihedrals	φ_0 (deg)	f_c (kJ mol ⁻¹)	X
H-C-S-O	0.0	0.8368	3
H-C-S-C	0.0	0.8368	3

VIII. Cartesian coordinates of all structures

Geometries of the optimal structures presented in Figs. 2 and 4 of the main text are listed below, with all coordinates in Angstroms.

Monomer

10

C	1.390750	0.279323	-0.278296
S	0.072728	-0.679506	0.585004
C	-1.342363	0.171624	-0.236526
O	0.075720	-0.189227	2.044957
H	1.346127	0.069130	-1.356470
H	1.227420	1.344812	-0.066434
H	2.347951	-0.053762	0.141464
H	-1.314193	-0.035613	-1.315827
H	-2.257159	-0.235280	0.211752
H	-1.256995	1.246897	-0.028367

D1

20

C	1.391830	0.296071	-0.267191
S	0.073035	-0.689518	0.555023
C	-1.343411	0.188626	-0.225497
O	0.078854	-0.256270	2.047129
H	1.379923	0.056354	-1.339642
H	1.179380	1.359143	-0.087564
H	2.341205	-0.018939	0.183566
H	-1.345350	-0.050790	-1.298081
H	-2.251051	-0.199163	0.253587
H	-1.209576	1.265306	-0.051326
S	-0.073081	3.587139	1.938615
O	-0.078682	3.153903	0.446506
C	-1.391839	2.601376	2.760682
C	1.343385	2.709142	2.719264
H	-1.380080	2.841096	3.833135
H	-2.341208	2.916257	2.309824
H	-1.179218	1.538334	2.581077
H	1.345162	2.948483	3.791865
H	1.209699	1.632459	2.545001
H	2.251033	3.097074	2.240313

D2
20

O	8.826895	8.110270	10.400227
S	9.972464	7.608129	9.483674
C	11.539269	7.974326	10.379345
H	12.382316	7.730081	9.717863
H	11.525836	9.039717	10.646509
H	11.551024	7.328890	11.266521
C	10.186293	8.892506	8.183524
H	11.035534	8.602394	7.548535
H	9.256912	8.900193	7.600878
H	10.362717	9.852789	8.687985
O	10.697510	11.161246	10.536141
S	9.253455	11.346438	11.076378
C	9.145789	10.330797	12.600760
H	8.213528	10.584098	13.124409
H	9.133390	9.289859	12.256910
H	10.027135	10.559985	13.215271
C	9.274676	12.983721	11.916622
H	8.313117	13.137349	12.426572
H	10.112562	12.992963	12.626663
H	9.422581	13.740250	11.136213

D3
20

C	-6.599507	-9.935427	-8.808258
S	-6.050826	-8.220930	-8.418528
C	-7.587463	-7.381111	-8.969174
O	-4.975044	-7.895873	-9.486073
H	-7.454125	-10.195223	-8.167596
H	-6.867985	-9.974321	-9.872589
H	-5.748550	-10.596439	-8.602335
H	-8.424339	-7.741197	-8.354184
H	-7.407231	-6.311806	-8.806702
H	-7.734957	-7.620273	-10.031201
S	-4.736135	-4.653480	-8.965041
O	-5.810347	-4.978975	-7.896071
C	-4.188088	-2.938502	-8.576590
C	-3.198394	-5.492320	-8.416137
H	-3.333958	-2.678643	-9.217880
H	-5.039455	-2.277959	-8.782326
H	-3.918996	-2.898989	-7.512438
H	-2.362832	-5.133640	-9.033730
H	-3.048402	-5.251363	-7.354870
H	-3.379470	-6.561814	-8.576431

D4

20

O	10.770543	12.406453	7.172925
S	10.996603	12.217603	8.692035
C	12.663048	11.452412	8.865018
H	12.827871	11.198932	9.921240
H	12.692858	10.559951	8.226519
H	13.389878	12.202747	8.531247
C	10.042817	10.713973	9.163143
H	10.255542	10.475201	10.214216
H	8.982319	10.960304	9.031380
H	10.346341	9.897937	8.494552
O	11.783311	8.009573	5.181466
S	11.481115	9.357691	5.867285
C	12.445813	10.642888	4.970928
H	12.145669	11.622494	5.364081
H	13.505277	10.435700	5.167309
H	12.228607	10.534564	3.900118
C	9.828399	9.903572	5.270228
H	9.653478	10.918986	5.647899
H	9.840437	9.858877	4.173228
H	9.097072	9.191144	5.672183

D5

20

C	0.832083	0.053205	0.687160
S	-0.018838	0.529481	-0.873482
S	1.568387	-2.573673	-1.989863
C	0.721902	-2.067199	-3.541948
C	-1.624708	-0.272902	-0.470355
O	-0.252453	2.053432	-0.806970
O	0.449839	-2.770887	-0.938584
C	2.024752	-4.266109	-2.547539
H	0.867295	-1.043176	0.726962
H	1.838413	0.487869	0.644560
H	0.262499	0.486055	1.520395
H	-1.455444	-1.355871	-0.418903
H	-1.978107	0.143628	0.482340
H	-2.317341	-0.012725	-1.280529
H	2.733390	-4.189503	-3.384114
H	2.491453	-4.765940	-1.690035
H	1.103863	-4.786018	-2.843846
H	1.450590	-2.071775	-4.364292
H	-0.098565	-2.774219	-3.724319
H	0.340792	-1.054444	-3.366810

T1
30

O	18.325573	19.811653	21.617481
S	19.721884	20.312996	21.169378
C	20.228323	21.608815	22.376809
H	21.215482	21.985848	22.075579
H	19.485068	22.415686	22.369997
H	20.289383	21.113897	23.353709
C	19.440363	21.463757	19.758658
H	20.418372	21.838813	19.426676
H	18.968548	20.870817	18.965678
H	18.799604	22.289633	20.091628
O	18.271096	24.146530	21.392567
S	17.718310	25.601134	21.478337
C	16.938575	25.747636	23.136233
H	16.505635	26.754394	23.216988
H	16.166283	24.969074	23.217754
H	17.742714	25.618895	23.871189
C	16.151632	25.602873	20.517245
H	15.714781	26.608754	20.587075
H	16.422965	25.376776	19.478677
H	15.486136	24.843390	20.952583
O	14.642326	23.527870	22.517495
S	15.116812	22.043647	22.457649
C	16.675088	21.971241	23.424806
H	17.142014	20.993610	23.248081
H	17.321498	22.778503	23.058847
H	16.399735	22.113636	24.476868
C	15.887654	21.824953	20.806281
H	16.405169	20.856910	20.796220
H	15.074819	21.866766	20.071118
H	16.603161	22.645493	20.671394

T2
30

C	19.978371	22.960022	19.710536
S	19.735892	23.242403	21.510328
C	20.388685	21.613064	22.058900
O	18.198954	23.189838	21.745112
C	15.358815	23.917374	20.096399
S	14.121084	23.111607	21.194225
C	15.047600	23.377434	22.762579
O	14.190395	21.590951	20.897064
S	17.054341	20.556144	20.208772
C	15.942352	19.217124	19.628149

O	18.501515	20.064915	19.893824
C	16.827935	20.251673	22.004302
H	21.059208	22.936455	19.512556
H	19.496985	22.004570	19.454354
H	19.514939	23.811524	19.197357
H	21.467010	21.591478	21.848409
H	20.210845	21.552465	23.139753
H	19.850741	20.831749	21.503192
H	15.760191	20.345461	22.229074
H	17.216281	19.244890	22.206490
H	17.413863	21.021960	22.516917
H	14.919373	19.492859	19.911972
H	16.052332	19.168894	18.537795
H	16.267612	18.274891	20.088960
H	15.332881	24.997756	20.296283
H	16.349231	23.496971	20.310933
H	15.040118	23.707847	19.068112
H	15.045690	24.454363	22.980238
H	14.504377	22.828117	23.541197
H	16.073387	23.010200	22.639216

T3

30

C	19.318080	22.762136	22.418743
S	18.401131	21.379365	21.618767
C	18.852818	21.822207	19.888771
O	16.894078	21.701134	21.778298
O	19.025390	25.162225	20.116170
S	18.978878	26.478380	19.285963
C	18.218864	27.737277	20.375610
C	20.695828	27.130948	19.340978
C	16.290257	24.915699	22.126303
S	15.070039	25.136098	20.770491
C	15.850747	23.953991	19.603056
O	15.323351	26.555016	20.184537
H	20.393691	22.575593	22.293887
H	19.028486	23.706104	21.941314
H	19.045684	22.740531	23.480909
H	19.921248	21.605360	19.751253
H	18.245550	21.181412	19.238001
H	18.646287	22.887366	19.725303
H	20.713003	28.127033	18.877545
H	21.008893	27.173273	20.392785
H	21.324967	26.432136	18.776249
H	18.326517	28.718024	19.891996
H	17.157993	27.455148	20.467183

H	18.745592	27.706182	21.339379
H	16.277900	23.860237	22.428986
H	17.274927	25.192098	21.728825
H	15.980785	25.581780	22.940796
H	15.862931	22.963479	20.077728
H	15.245255	23.967205	18.688986
H	16.872837	24.307564	19.416185

T4

30

C	5.071517	-0.034670	-3.655985
S	4.287297	-0.194668	-1.997307
C	5.830416	-0.559251	-1.075361
O	3.893217	1.257561	-1.611793
S	-0.020529	2.540318	0.295084
C	1.283159	3.066414	-0.885371
O	0.572434	2.732177	1.715202
C	3.644181	1.756288	1.598188
S	2.617946	0.269497	1.276626
C	1.964214	0.086045	2.982365
O	3.615924	-0.905124	1.078908
H	1.323627	0.953582	3.183548
H	1.388114	-0.847471	2.998202
H	2.818493	0.022048	3.669544
H	2.968760	2.565559	1.900207
H	4.362207	1.495270	2.386815
H	4.148555	1.979398	0.651252
H	0.822989	3.182558	-1.876460
H	1.688760	4.020594	-0.522132
H	2.057413	2.289562	-0.920766
H	5.497260	-1.005416	-3.946611
H	4.282043	0.264332	-4.356496
H	5.846821	0.740863	-3.594728
H	6.247662	-1.502562	-1.454190
H	6.520679	0.279922	-1.237121
H	5.523931	-0.655551	-0.027295
C	-1.126902	3.988674	0.041019
H	-1.509237	3.972861	-0.989222
H	-1.948976	3.889460	0.760368
H	-0.546405	4.899313	0.241051

T5

30

O	16.634857	24.592189	18.933949
S	17.819686	24.188608	19.842340
C	18.546611	25.748060	20.487096
H	19.438384	25.480875	21.069767
H	18.776646	26.394312	19.630220
H	17.780785	26.213377	21.119207
C	19.237765	23.746631	18.763679
H	20.096423	23.565749	19.425082
H	18.955755	22.836787	18.219781
H	19.417204	24.574596	18.065138
O	20.209226	23.485765	22.163446
S	18.877554	23.104769	22.864853
C	19.254372	22.812446	24.636229
H	18.324234	22.468296	25.107880
H	20.058270	22.067975	24.708308
H	19.577739	23.772502	25.056335
C	18.574534	21.347602	22.430705
H	17.751416	20.981712	23.056223
H	18.299881	21.331231	21.369829
H	19.512448	20.803987	22.601658
O	15.856035	22.403783	23.805490
S	15.408064	22.687282	22.347855
C	15.384240	24.514743	22.152187
H	15.163099	24.748814	21.101020
H	14.647435	24.936357	22.847504
H	16.395863	24.844707	22.412702
C	13.585634	22.453003	22.322482
H	13.200021	22.813677	21.358789
H	13.395364	21.379488	22.440968
H	13.163459	23.017678	23.164279

T6

30

O	18.248791	19.538962	25.445555
S	18.177691	19.442715	26.988687
C	18.433034	21.156221	27.613792
H	18.496857	21.127477	28.710183
H	19.356533	21.546423	27.166533
H	17.561677	21.740741	27.294830
C	19.813685	18.792657	27.529990
H	19.853766	18.804080	28.627823
H	19.884199	17.765020	27.153619
H	20.593531	19.428978	27.091708

O	22.122928	22.013981	19.259183
S	22.029013	21.907157	20.795300
C	22.263129	23.603652	21.467768
H	22.337954	23.520943	22.560161
H	23.173825	24.017982	21.015392
H	21.385740	24.187672	21.162752
C	23.639059	21.242274	21.387621
H	23.636418	21.292751	22.484521
H	23.704654	20.207811	21.027740
H	24.435317	21.852934	20.941810
O	22.288179	21.938705	24.307074
S	21.002813	21.173364	24.716842
C	20.992990	19.611911	23.748124
H	20.049272	19.097423	23.964572
H	21.091252	19.874277	22.687275
H	21.857084	19.027672	24.087681
C	19.609864	21.978664	23.829299
H	18.704772	21.397957	24.043202
H	19.535878	22.999435	24.224070
H	19.855097	21.990158	22.759892

T7

30

C	0.472180	-0.265895	0.733682
S	-0.136458	0.321670	-0.898489
O	-0.384447	1.846400	-0.754727
C	-1.785515	-0.482541	-0.798695
O	0.359320	-2.893610	-1.176365
S	1.641205	-2.693731	-2.021010
C	2.115524	-4.372107	-2.603230
C	1.077057	-2.055772	-3.650613
H	0.551026	-1.358283	0.675742
H	1.451728	0.200982	0.892637
H	-0.247228	0.058360	1.495983
H	-1.625451	-1.566818	-0.828784
H	-2.261186	-0.155086	0.134675
H	-2.355211	-0.137931	-1.670337
H	2.951015	-4.283369	-3.311612
H	2.420451	-4.939134	-1.715311
H	1.234961	-4.831777	-3.071533
H	1.927235	-2.048859	-4.346467
H	0.268384	-2.708093	-4.006330
H	0.713231	-1.036965	-3.472756
S	-2.320128	1.993864	2.169713
O	-3.154515	2.294445	3.432453
C	-3.077491	2.942538	0.787412

C	-0.788980	3.007148	2.285051
H	-2.419933	2.841894	-0.086210
H	-4.064898	2.499581	0.606587
H	-3.180753	3.985061	1.116591
H	-0.254575	2.912504	1.330540
H	-1.090007	4.041603	2.496975
H	-0.204794	2.601451	3.120616

T8

30

O	22.134918	25.903523	23.940447
S	23.041269	24.808338	24.561304
C	22.070844	24.071469	25.935851
H	22.726180	23.402398	26.509576
H	21.686789	24.890733	26.558087
H	21.251172	23.507444	25.474200
C	24.246540	25.712157	25.614598
H	24.837479	24.984221	26.187314
H	24.891884	26.286350	24.938904
H	23.682050	26.382530	26.276309
O	18.026224	22.657810	23.136880
S	19.327282	23.413547	23.474273
C	18.847931	25.002640	24.270183
H	19.769957	25.568621	24.458552
H	18.190563	25.554032	23.588146
H	18.338681	24.736761	25.204821
C	19.960394	24.149959	21.912549
H	20.865655	24.718669	22.164650
H	20.186067	23.308764	21.246021
H	19.190316	24.810736	21.496604
O	18.606089	27.152941	21.810753
S	19.594310	28.340832	21.800217
C	21.206535	27.678398	21.199666
H	21.938315	28.498325	21.206754
H	21.524346	26.861633	21.859709
H	21.033168	27.327994	20.175000
C	20.127602	28.590982	23.547016
H	20.862715	29.407639	23.569519
H	19.226795	28.869318	24.107320
H	20.565929	27.657234	23.920780

References

- [S1] *CRC Handbook of Chemistry and Physics*, 99th ed. (Ed.: J. R. Rumble), CRC Press, Boca Raton, **2018**.
- [S2] D. Hait, M. Head-Gordon, *J. Chem. Theory Comput.* **2018**, *14*, 1969.
- [S3] M. J. Frisch, G. W. Trucks, H. B. Schlegel, G. E. Scuseria, M. A. Robb, J. R. Cheeseman, G. Scalmani, V. Barone, B. Mennucci, G. A. Petersson, H. Nakatsuji, M. Caricato, X. Li, H. P. Hratchian, A. F. Izmaylov, J. Bloino, G. Zheng, J. L. Sonnenberg, M. Hada, M. Ehara, K. Toyota, R. Fukuda, J. Hasegawa, M. Ishida, T. Nakajima, Y. Honda, O. Kitao, H. Nakai, T. Vreven, J. A. Montgomery, Jr., J. E. Peralta, F. Ogliaro, M. Bearpark, J. J. Heyd, E. Brothers, K. N. Kudin, V. N. Staroverov, R. Kobayashi, J. Normand, K. Raghavachari, A. Rendell, J. C. Burant, S. S. Iyengar, J. Tomasi, M. Cossi, N. Rega, J. M. Millam, M. Klene, J. E. Knox, J. B. Cross, V. Bakken, C. Adamo, J. Jaramillo, R. Gomperts, R. E. Stratmann, O. Yazyev, A. J. Austin, R. Cammi, C. Pomelli, J. W. Ochterski, R. L. Martin, K. Morokuma, V. G. Zakrzewski, G. A. Voth, P. Salvador, J. J. Dannenberg, S. Dapprich, A. D. Daniels, Ö. Farkas, J. B. Foresman, J. V. Ortiz, J. Cioslowski, D. J. Fox, *Gaussian 09, rev. D.01*, Gaussian, Inc., Wallingford (CT), **2009**.
- [S4] B. Aradi, B. Hourahine, Th. Frauenheim, *J. Phys. Chem. A.* **2007**, *111*, 5678.
- [S5] M. L. Strader, S. E. Feller, *J. Phys. Chem. A.* **2002**, *106*, 1074.
- [S6] A. Barducci, M. Bonomi, M. Parrinello, *WIREs Comput. Mol. Sci.* **2011**, *1*, 826.
- [S7] M. J. Abraham, T. Murtola, R. Schulz, S. Páll, J. C. Smith, B. Hess, E. Lindahl, *SoftwareX* **2015**, *1-2*, 19.
- [S8] G. A. Tribello, M. Bonomi, D. Branduardi, C. Camilloni, G. Bussi, *Comput. Phys. Commun.* **2014**, *185*, 604.
- [S9] H. Jonson, G. Mills, K. W. Jacobsen, in *Classical and Quantum Dynamics in Condensed Phase Simulations* (Eds.: B. J. Berne, G. Ciccotti, D. F. Coker, D. F.), World Scientific, Singapore, **1998**, pp. 385-404.
- [S10] TeraChem v 1.9. <http://www.petachem.com>.
- [S11] I. S. Ufimtsev, T. J. Martinez, *J. Chem. Theory Comput.* **2009**, *5*, 2619.